

Folding State within a Hysteresis Loop: Hidden Multistability in Nonlinear Physical Systems


Meng-Xia Bi^{1,*}, Huawei Fan^{1,*}, Xiao-Hong Yan^{2,†} and Ying-Cheng Lai^{3,4}

¹*School of Science, Xi'an University of Posts and Telecommunications, Xi'an 710121, China*

²*School of Material Science and Engineering, Jiangsu University, Zhenjiang 212013, China*

³*School of Electrical, Computer, and Energy Engineering, Arizona State University, Tempe, Arizona 85287, USA*

⁴*Department of Physics, Arizona State University, Tempe, Arizona 85287, USA*

 (Received 25 June 2023; revised 28 November 2023; accepted 12 February 2024; published 25 March 2024)

Identifying hidden states in nonlinear physical systems that evade direct experimental detection is important as disturbances and noises can place the system in a hidden state with detrimental consequences. We study a cavity magnonic system whose main physics is photon and magnon Kerr effects. Sweeping a bifurcation parameter in numerical experiments (as would be done in actual experiments) leads to a hysteresis loop with two distinct stable steady states, but analytic calculation gives a third folded steady state “hidden” in the loop, which gives rise to the phenomenon of hidden multistability. We propose an experimentally feasible control method to drive the system into the folded hidden state. We demonstrate, through a ternary cavity magnonic system and a gene regulatory network, that such hidden multistability is in fact quite common. Our findings shed light on hidden dynamical states in nonlinear physical systems which are not directly observable but can present challenges and opportunities in applications.

DOI: [10.1103/PhysRevLett.132.137201](https://doi.org/10.1103/PhysRevLett.132.137201)

Bistability is referred to as the coexistence of two distinct steady states in the system. As a bifurcation parameter sweeps forward and backward through a range, different steady states appear, leading to a hysteresis loop. Bistability or even multistability is ubiquitous in nonlinear dynamical systems [1–3]. For example, in physics and engineering, bistability and multistability have applications in computing and information processing devices such as switches, memories, and logic gates [4–9]. In systems and synthetic biology, the dynamics of gene regulatory networks are typically bistable with a healthy state and a cancerous state [10–12]. In neuroscience, multistability is fundamental to the functioning of the brain network [13,14]. In ecological networks, bistable dynamics leading to a tipping point transition from a survival to an extinction state is of great concern [15–18]. When investigating bistability for applications, a tacit assumption is that the system has only two steady states, on which experimental designs and observations depend.

What if, in the bistable regime, there is a third, “hidden” steady state in the system that cannot be experimentally revealed by sweeping some parameter forward and backward? The existence of such a hidden state can be concerning. For example, if a device is designed and experimentally tested in the laboratory to operate based on the known two coexisting steady states (e.g., as a physical memory or other binary devices), then significant errors can arise when the device is deployed to real-world applications where noise “kicks” the system into the basin of attraction of the hidden state. Can such a scenario arise in natural systems? If yes, it

will be essential to conduct experimental tests to assess the possible existence of the hidden state.

In this Letter, we present a class of systems that indeed host a hidden state folding in the hysteresis loop in the regime of bistability. For convenience, we use term “hidden multistability” to describe the associated phenomenon caused by the folded hidden state (FHS). Our prototypical model is a cavity magnonic system with photon and magnon Kerr effects. Analytic solutions are obtained, revealing an FHS. However, numerical simulations with continuous parameter sweeping (as in a standard experimental test) absolutely fail to reveal the FHS inside the hysteresis loop. We propose an experimentally feasible scheme based on rectangular-pulse control signals to detect the FHS. We also report two additional systems that exhibit hidden multistability: a ternary cavity magnonic system and a gene regulatory network. As bistability and hysteresis loops are ubiquitous in physical and biological systems with applications in information storage and processing, our Letter highlights the importance of ascertaining the existence (or nonexistence) of FHS that can potentially cause the system to produce unanticipated and undesired behaviors.

Cavity magnonic systems [19–52] are a class of hybrid light-matter interacting systems in which a ferromagnetic insulator such as yttrium iron garnet (YIG) crystal embedded in a microwave cavity coherently [20–23] or dissipatively [29–32] couples to photons. Experimental and theoretical studies [33–52] provided the foundation for this class of systems to be exploited for information processing

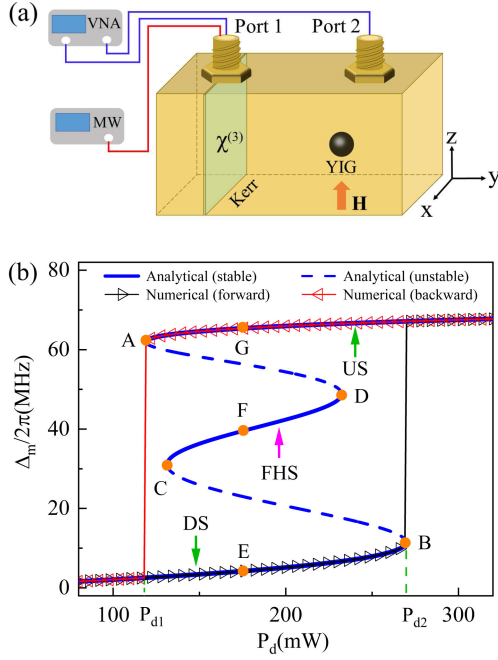


FIG. 1. Schematic illustration of the cavity magnonic system and nonlinear steady-state dynamic behaviors of the system. (a) A YIG sphere and a Kerr medium are embedded in a microwave cavity. The microwave transmission is measured by a VNA via ports 1 and 2, and the cavity photons are strongly driven by an MW via port 1. The YIG sphere is placed in a uniformly biased magnetic field \mathbf{H} that aligns the magnetization and tunes the magnon frequency. (b) Theoretically predicted and numerically calculated magnon frequency shift $\Delta_m/2\pi$ versus the driving power P_d for $\omega_d/2\pi = 10.038$ GHz. The black and red triangle curves, respectively, correspond to the forward and backward sweeps of the driving power P_d . The blue solid and dashed curves, respectively, denote the analytically obtained stable and unstable steady states.

and storage applications. In addition, strong driving can amplify the magnetocrystalline anisotropy of the YIG crystal, generating the magnon Kerr effect [53] and making the hybrid system a nonlinear system with bistability and a hysteresis loop [54–56]. Depending on the direction of the external magnetic field along the crystal axis, the induced magnon Kerr effect can be either positive or negative, affecting the orientation of the hysteresis loop. If the system has two cavities [57,58], is non-Hermitian [59–63], or is subject to mechanical vibrations [64], rich phenomena such as nonreciprocal transmission, ultralow threshold bistability, enhancement of high-order sidebands and detection sensitivity, and mechanical bistability can arise. When multiple YIG crystals or alternative nonlinear effects are present, the hybrid system can exhibit multistability [65–67]. These previous studies established the nonlinear cavity magnonic systems as a promising platform for switches, memories, logic gates, and detectors.

Figure 1(a) illustrates the system configuration: a microwave cavity contains a YIG sphere with magnetocrystalline

anisotropy and a Kerr medium with third-order nonlinear susceptibility $\chi^{(3)}$. A microwave probe field generated by a vector network analyzer (VNA) is injected into the cavity from port 1 and comes out from port 2 for microwave transmission to be measured. A microwave pump field generated by a microwave source (MW) provides strong driving to the cavity photons via port 1. In addition, a uniformly biased magnetic field \mathbf{H} along the z direction is applied to the YIG sphere to align its magnetization and tune the frequency of the magnon mode. Here we focus on the typical Kittel mode in which all spins uniformly precess in phase under the uniformly biased magnetic field.

The Hamiltonian taking into account the photon and magnon Kerr effects is (see Sec. I in Supplemental Material [68]) $H = \omega_c a^\dagger a + \omega_m m^\dagger m + K_a a^\dagger a a^\dagger a + K_m m^\dagger m m^\dagger m + g(a^\dagger m + a m^\dagger) + \Omega_d(a^\dagger e^{-i\omega_d t} + a e^{i\omega_d t}) + \eta(a^\dagger e^{-i\omega_p t} + a e^{i\omega_p t})$, where a^\dagger and a (m^\dagger and m), respectively, are the photon (magnon) creation and annihilation operators with frequency ω_c (ω_m), $K_{a(m)}$ is the photon (magnon) Kerr coefficient, g is the interaction strength between photon and magnon, Ω_d (η) and ω_d (ω_p) are the driving field (probe field) strength and frequency, respectively. The driving power P_d is chosen to be the bifurcation parameter, which is related to Ω_d as $\Omega_d = \sqrt{P_d \kappa_{c1} / (\hbar \omega_d)}$, where \hbar is the Planck constant, and κ_{c1} is the external photon dissipation rate through port 1 in Fig. 1(a). Employing the quantum Langevin method [69] to the Hamiltonian and expressing the operators a and m each as a sum of the expectation values and fluctuations: $a = \langle a \rangle + \delta a$ and $m = \langle m \rangle + \delta m$, we obtain the equations of motion in terms of the amplitudes A_d and M_d of the expectation values resulting from the driving field (Sec. II in Supplemental Material [68]):

$$\begin{aligned} \dot{A}_d &= -i \left[\left(\delta_c + \Delta_a - i \frac{\kappa_c}{2} \right) A_d + g M_d + \Omega_d \right], \\ \dot{M}_d &= -i \left[\left(\delta_m + \Delta_m - i \frac{\gamma_m}{2} \right) M_d + g A_d \right], \end{aligned} \quad (1)$$

where $\delta_{c(m)} \equiv \omega_{c(m)} - \omega_d$ is the photon (magnon) frequency detuning relative to the driving-field frequency, κ_c (γ_m) is the dissipation rate of the photon (magnon), $\Delta_a = 2K_a |A_d|^2$ and $\Delta_m = 2K_m |M_d|^2$ are the respective frequency shifts due to the photon and magnon Kerr effects. The steady states can be obtained by setting $\dot{A}_d = 0$ and $\dot{M}_d = 0$, resulting in a higher-order nonlinear equation for Δ_m :

$$\begin{aligned} \left[\delta_c + \frac{K_a \Gamma_m \Delta_m}{K_m g^2} - \frac{g^2 (\delta_m + \Delta_m)}{\Gamma_m} \right]^2 \Gamma_m \Delta_m \\ + \left(\frac{\kappa_c}{2} + \frac{g^2 \gamma_m / 2}{\Gamma_m} \right)^2 \Gamma_m \Delta_m - 2K_m \Omega_d^2 g^2 = 0, \end{aligned} \quad (2)$$

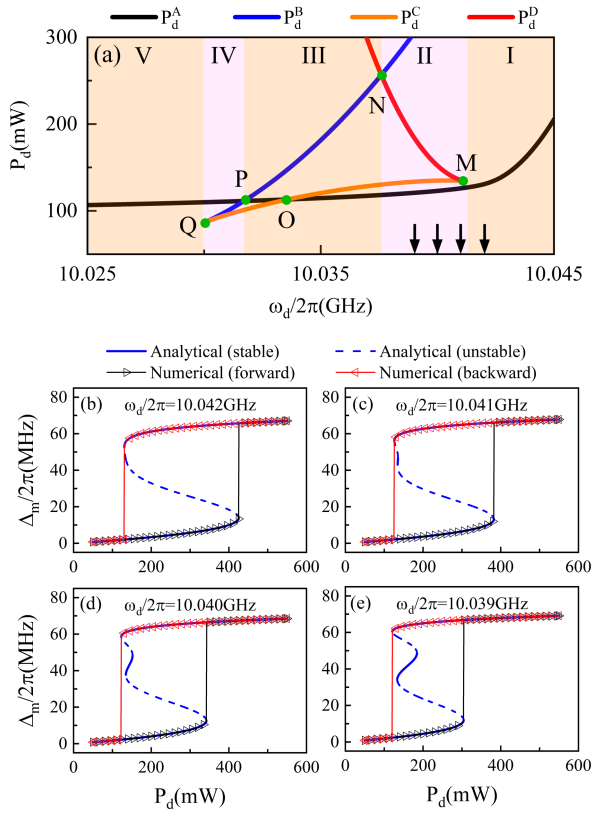


FIG. 2. Distinct dynamical regimes and hysteresis loops. (a) Driving powers P_d^{A-D} at the switching points versus the driving frequency $\omega_d/2\pi$. Regions I–V correspond to bistability, hidden multistability, multistability, two bistability, and again bistability, respectively. The four vertical downward black arrows from left to right denote the frequency values $\omega_d/2\pi = 10.039$, 10.040, 10.041, and 10.042 GHz, respectively. (b)–(e) Hysteresis loops with or without an FHS for these four frequency values.

where $\Gamma_m \equiv (\delta_m + \Delta_m)^2 + \gamma_m^2/4$. Note that Eq. (2) contains both the magnon and photon Kerr effects. A method for determining the stability of the solutions Δ_m in Eq. (2) can be found in Sec. II of Supplemental Material [68]. Typical parameter values are $\omega_c/2\pi = 10.08$ GHz, $\omega_m/2\pi = 10.047$ GHz, $g/2\pi = 40$ MHz, $K_m/2\pi = 9.8$ nHz, $K_a/2\pi = -0.98$ nHz, $\kappa_c/2\pi = 1.5$ MHz, $\kappa_{c1}/2\pi = 1.0$ MHz, and $\gamma_m/2\pi = 16.5$ MHz.

As the driving power P_d increases from zero, the photon and magnon Kerr nonlinearities are turned on and dominate the dynamics. Figure 1(b) shows the numerical and analytical magnon frequency shift $\Delta_m/2\pi$ versus P_d for $\omega_d/2\pi = 10.038$ GHz, where the numerical experiments are conducted by slowly sweeping forward (black triangles) and backward (red triangles) the bifurcation parameter P_d at the step size $\delta P_d = 0.1$ mW. The numerical results reveal bistability with a counterclockwise hysteresis loop. Surprisingly, the analysis of Eq. (2) gives different results: in addition to the hysteresis loop that agrees well with the numerics, there is a third, FHS, as indicated by the blue solid curve inside the loop.

The dynamical mechanism for the emergence of a hysteresis loop can be described, as follows. Let DS (US) denote the down (up) steady state that exists for $P_d < P_{d2}$ ($P_d > P_{d1}$), as shown in Fig. 1(b). Since $P_{d1} < P_{d2}$, the DS and US coexist in the parameter interval $[P_{d1}, P_{d2}]$, each with its own basin of attraction. As P_d increases from a value less than P_{d1} at which the DS is the only steady state in the system, what is observed is the DS, until P_d reaches P_{d2} where the DS disappears and its basin of attraction is absorbed into that of the US. There is then a sudden switch from the DS to the US at P_{d2} . For $P_d > P_{d2}$, the US is the experimentally observed steady state. Likewise, when P_d decreases from a value greater than P_{d2} , the observed steady state is the US until P_{d1} is reached, at which the US is destroyed, leaving the DS the only steady state in the system. The observable steady state switches from the US to the DS as P_d decreases through P_{d1} . A hysteresis loop then arises in the parameter interval $[P_{d1}, P_{d2}]$, in which the DS and US coexist.

The question is whether an FHS, if it indeed exists, can be observed by sweeping a bifurcation parameter forward and backward. The answer is negative. As shown in Fig. 1(b), in both sweeping directions, the observed steady state is either the DS or US, but never the FHS. That is, in spite of having a nonzero basin of attraction (Fig. S2 in Supplemental Material [68]), the third folded steady state remains hidden, regardless of the direction of parameter sweeping. The phenomenon in Fig. 1(b) caused by FHS can be called hidden multistability.

To study the formation process of the hidden multistability, four switching points, A – D , are specified in Fig. 1(b), at which the magnon frequency changes abruptly. Figure 2(a) shows the driving power P_d^{A-D} of the switching points versus the driving frequency $\omega_d/2\pi$, leading to five distinct regions: I–V from right to left. In each region, there are more than one steady state, but not every one of them can be revealed by numerically or experimentally sweeping a parameter forward and backward. In region I, P_d^A (black curve) and P_d^B (blue curve, $P_d^B > 300$ mW—beyond the scale of the plot) exist with $P_d^A < P_d^B$, so there is bistability. As the driving frequency $\omega_d/2\pi$ decreases, P_d^C (orange curve) and P_d^D (red curve) emerge at the point M . As the driving power P_d is swept, the observed states are P_d^A and P_d^B , respectively, forming a hysteresis loop, inside which P_d^C and P_d^D are hidden ($[P_d^C, P_d^D] \subset [P_d^A, P_d^B]$). There is then hidden multistability in region II. As P_d^D increases, at point N , it becomes equal to P_d^B —the beginning of region III, where the inequality $P_d^A < P_d^C < P_d^B < P_d^D$ holds. In this case, for forward parameter sweeping, the US, middle stable state, and the DS can be observed but for backward sweeping, only the US and DS come out [Fig. S3(a) in Supplemental Material [68]], signifying multistability. As $\omega_d/2\pi$ continues to decrease to the point O , the inequality $P_d^C < P_d^A < P_d^B < P_d^D$ emerges and there is again

multistability [Fig. S3(b) in Supplemental Material [68]]. At point P , the system enters into region IV where $P_d^C < P_d^B < P_d^A < P_d^D$ holds and there is two bistability. In this case, two independent bistable loops arise [Fig. S3(c) in Supplemental Material [68]]. At point Q , P_d^B , and P_d^C merge and disappear, and the system enters into region V with $P_d^A < P_d^D$ (note that the latter is out of the scale of the figure), producing again bistability [Fig. S3(d) in Supplemental Material [68]]. While an FHS cannot be directly accessed due to its hidden nature, Fig. 2(a) suggests a general approach to predicting and understanding hidden multistability in nonlinear systems by monitoring the variational trend of the hysteresis loop associated with the switching point.

From region I to region II, there is a continuous transition from bistability to hidden multistability with similar numerical results. To better understand this transition, we choose four values of the driving frequency $\omega_d/2\pi$, as indicated by the downward arrows in Fig. 2(a), and calculate both numerically and analytically the magnon frequency shift $\Delta_m/2\pi$ versus the driving power P_d , as shown in Figs. 2(b)–2(e), respectively. For $\omega_d/2\pi = 10.042$ GHz, the system is in region I and exhibits bistability in both numerical and analytical results in Fig. 2(b). As the system moves into region II, numerical calculations still reveal bistability, but the analytic results show that another new stable state (i.e., FHS) is generated in the hysteresis loop, leading to hidden multistability, as shown in Figs. 2(c)–2(e). This continuous transition without any indicators in numerical simulations (or experimental test) inevitably may lead to the erroneous conclusion that the system exhibits bistability (not hidden multistability).

To reveal the FHS inside the hysteresis loop in Fig. 1(b) requires the application of some control strategy [75]. It is desired to have an efficient, experimentally readily implementable method with low cost. Here we exploit a rectangular-pulse control method [76,77] for detecting the FHS. In particular, we consider the following rectangular-pulse driving field: $P_d = P_0 \pm P_l[u(t - t_0) - u(t - t_0 - \Delta t)]$, where “ \pm ” corresponds to the forward and reverse pulses, respectively, P_0 is the initial power, P_l is the height (depth) of the forward (reverse) pulse, $u(t - \tau)$ ($\tau = t_0$ or $t_0 + \Delta t$) is the Heaviside function: $u(t - \tau) = 0$ for $t < \tau$ and $u(t - \tau) = 1$ for $t \geq \tau$, and Δt is the duration of the pulse. Figure 3(a) shows an example of the forward pulse for $P_0 = 175$ mW, $P_l = 125$ mW, $t_0 = 1$ μ s, and $\Delta t = 1$ μ s. Figure 3(b) shows the time evolution of the magnon frequency shift $\Delta_m/2\pi$ under the forward pulse. Initially, the system is in the DS corresponding to point E in Fig. 1(b). During the time when the pulse is applied, $\Delta_m/2\pi$ increases. When the pulse is removed at $t = 2$ μ s, $\Delta_m/2\pi$ begins to decrease slightly and then stabilizes at a constant value associated with the FHS [corresponding to point F in Fig. 1(b)] after $t \gtrsim 3$ μ s. Similarly, for the reverse pulse shown in Fig. 3(c) where $P_0 = 175$ mW, $P_l = 75$ mW, $t_0 = 1$ μ s, and $\Delta t = 1$ μ s, the system is initially in the US

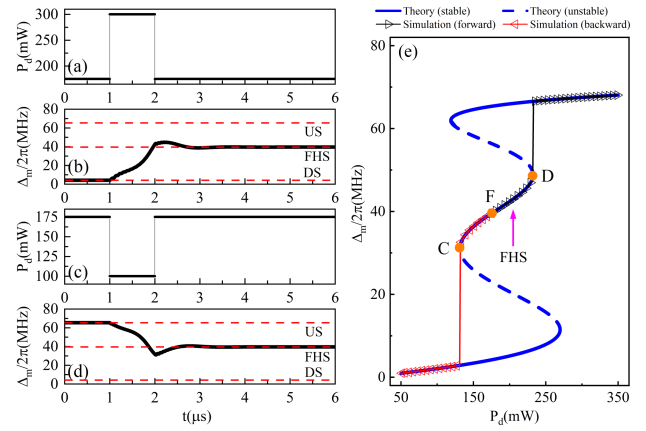


FIG. 3. Detecting FHS numerically (or experimentally) through application of a suitable control driving pulse. (a) Forward control pulse with parameters $P_0 = 175$ mW, $P_l = 125$ mW, $t_0 = 1$ μ s, and $\Delta t = 1$ μ s. (b) Time evolution of the system into the FHS. (c),(d) Similar to (a),(b) but for reversed-pulse control with parameters $P_0 = 175$ mW, $P_l = 75$ mW, $t_0 = 1$ μ s, and $\Delta t = 1$ μ s. (e) Sweep of the FHS for system initiated at point F in Fig. 1(b).

[point G in Fig. 1(b)] and $\Delta_m/2\pi$ decreases when the control pulse starts. To make the system evolve into the FHS, we terminate the pulse at $t = 2$ μ s. After a short transient, the system stabilizes at the FHS [point F in Fig. 1(b)], as shown in Fig. 3(d). (See Fig. S4 in Supplemental Material [68] for more details.) If the system is initialized at point F in Fig. 1(b), a continuous forward or backward sweeping of the driving can reveal the entire FHS between points C and D , as shown in Fig. 3(e). Through control, the FHS can effectively serve as a rapid transition platform between the DS and US. Theoretically, the control method to “force” the system into the FHS can be also justified through the transmission coefficient (Sec. VI in Supplemental Material [68]).

To summarize, through analytic derivation and numerical experiments, we have uncovered the phenomenon of hidden multistability in a nonlinear cavity magnonic system, whereby the system possesses multistability but one state is hidden in the sense that the system is unable to land on it through continuous sweeping of a bifurcation parameter, so a routine numerical or experimental study would conclude, erroneously, that the system is bistable. We have identified the route from bistability to hidden multistability based on the variational trend of the hysteresis loop associated with the switching point, and articulated an experimentally feasible strategy to reveal the FHS by driving the system into it through a suitable control pulse. (See Sec. VII in Supplemental Material [68] for a full treatment of the effects of noise on FHS and control.) Moreover, the hidden multistability has been verified in other nonlinear physical and biological systems such as a ternary cavity magnonic system and a gene regulatory network (Sec. VIII in Supplemental Material [68]). In addition, the hidden state within the hysteresis loop can be a

chaotic attractor in some parameter regime of the ternary cavity magnonic system (exemplified in Fig. S8 and treated in Supplemental Material [68]).

The FHS uncovered here has significant real-world implications and applications. For example, it has been known that bistability and hysteresis loops are fundamental to information storage and processing in physical and biological systems. For an information system designed based on bistability, the occurrence of an FHS can potentially lead to failures, rendering important to ensure that such a hidden state does not arise in the parameter regime of operation for the intended applications. From a different perspective, the hidden nature of an FHS makes it a potential candidate for information encryption, especially because switching to the FHS containing the desired information can be fast at a low energy cost.

The FHS reported in this Letter is different from a hidden attractor [78] whose basin of attraction has no intersection with the unstable manifold of an unstable fixed point [78]. In our Letter, the FHS is related to the operation of cavity magnonic system experiment and is responsible for a continuous transition from bistability to hidden multistability. The lack of any indicator in numerical simulation or experimental test associated with this transition was the main reason that the FHS had been overlooked in previous works on bistability and hysteresis loops.

While we have uncovered and characterized hidden multistability in a cavity magnonic system, a theory that is generally applicable to diverse nonlinear systems for identifying and understanding FHS is needed. Realizing experimental control to drive the system into an FHS remains to be seen. Exploiting hidden multistability for information processing is also worthy.

This work was supported by the National Natural Science Foundation of China (NNSFC) (Grants No. 12204374, No. 12105165, and No. 12174158) and the National Key Research and Development Program of China (Grant No. 2022YFA1405200). Y.C.L. was supported by AFOSR under Grant No. FA9550-21-1-0438.

*These authors contributed equally to this work.

†yanxh@ujs.edu.cn

- [1] U. Feudel, Complex dynamics in multistable systems, *Int. J. Bifurcation Chaos Appl. Sci. Eng.* **18**, 1607 (2008).
- [2] A. N. Pisarchik and U. Feudel, Control of multistability, *Phys. Rep.* **540**, 167 (2014).
- [3] U. Feudel, A. N. Pisarchik, and K. Showalter, Multistability and tipping: From mathematics and physics to climate and brain: Minireview and preface to the focus issue, *Chaos* **28**, 033501 (2018).
- [4] C. Argyropoulos, P.-Y. Chen, F. Monticone, G. D'Aguanno, and A. Alù, Nonlinear plasmonic cloaks to realize giant all-optical scattering switching, *Phys. Rev. Lett.* **108**, 263905 (2012).
- [5] J. Sheng, U. Khadka, and M. Xiao, Realization of all-optical multistate switching in an atomic coherent medium, *Phys. Rev. Lett.* **109**, 223906 (2012).
- [6] C. K. Andersen and K. Mølmer, Circuit QED flip-flop memory with all-microwave switching, *Phys. Rev. Appl.* **3**, 024002 (2015).
- [7] V. Bacot, S. Perrard, M. Labousse, Y. Couder, and E. Fort, Multistable free states of an active particle from a coherent memory dynamics, *Phys. Rev. Lett.* **122**, 104303 (2019).
- [8] Y. Tadokoro and H. Tanaka, Highly sensitive implementation of logic gates with a nonlinear nanomechanical resonator, *Phys. Rev. Appl.* **15**, 024058 (2021).
- [9] R. Fermin, N. M. A. Scheinowitz, J. Aarts, and K. Lahabi, Mesoscopic superconducting memory based on bistable magnetic textures, *Phys. Rev. Res.* **4**, 033136 (2022).
- [10] M. Wu, R.-Q. Su, X.-H. Li, T. Ellis, Y.-C. Lai, and X. Wang, Engineering of regulated stochastic cell fate determination, *Proc. Natl. Acad. Sci. U.S.A.* **110**, 10610 (2013).
- [11] L.-Z. Wang, R.-Q. Su, Z.-G. Huang, X. Wang, W.-X. Wang, C. Grebogi, and Y.-C. Lai, A geometrical approach to control and controllability of nonlinear dynamical networks, *Nat. Commun.* **7**, 11323 (2016).
- [12] F.-Q. Wu, R.-Q. Su, Y.-C. Lai, and X. Wang, Engineering of a synthetic quadrastable gene network to approach Waddington landscape and cell fate determination, *eLife* **6**, e23702 (2017).
- [13] G. Deco and V. K. Jirsa, Ongoing cortical activity at rest: Criticality, multistability, and ghost attractors, *J. Neurosci.* **32**, 3366 (2012).
- [14] J. A. S. Kelso, Multistability and metastability: Understanding dynamic coordination in the brain, *Phil. Trans. R. Soc. B* **367**, 906 (2012).
- [15] J. Jiang, Z.-G. Huang, T. P. Seager, W. Lin, C. Grebogi, A. Hastings, and Y.-C. Lai, Predicting tipping points in mutualistic networks through dimension reduction, *Proc. Natl. Acad. Sci. U.S.A.* **115**, E639 (2018).
- [16] J. Jiang, A. Hastings, and Y.-C. Lai, Harnessing tipping points in complex ecological networks, *J. R. Soc. Interface* **16**, 20190345 (2019).
- [17] Y. Meng, J. Jiang, C. Grebogi, and Y.-C. Lai, Noise-enabled species recovery in the aftermath of a tipping point, *Phys. Rev. E* **101**, 012206 (2020).
- [18] Y. Meng, Y.-C. Lai, and C. Grebogi, Tipping point and noise-induced transients in ecological networks, *J. R. Soc. Interface* **17**, 20200645 (2020).
- [19] Ö. O. Soykal and M. E. Flatté, Strong field interactions between a nanomagnet and a photonic cavity, *Phys. Rev. Lett.* **104**, 077202 (2010).
- [20] H. Huebl, C. W. Zollitsch, J. Lotze, F. Hocke, M. Greifenstein, A. Marx, R. Gross, and S. T. B. Goennenwein, High cooperativity in coupled microwave resonator ferrimagnetic insulator hybrids, *Phys. Rev. Lett.* **111**, 127003 (2013).
- [21] Y. Tabuchi, S. Ishino, T. Ishikawa, R. Yamazaki, K. Usami, and Y. Nakamura, Hybridizing ferromagnetic magnons and microwave photons in the quantum limit, *Phys. Rev. Lett.* **113**, 083603 (2014).
- [22] X. Zhang, C.-L. Zou, L. Jiang, and H. X. Tang, Strongly coupled magnons and cavity microwave photons, *Phys. Rev. Lett.* **113**, 156401 (2014).

- [23] D. Zhang, X.-M. Wang, T.-F. Li, X.-Q. Luo, W. Wu, F. Nori, and J. You, Cavity quantum electrodynamics with ferromagnetic magnons in a small yttrium-iron-garnet sphere, *npj Quantum Inf.* **1**, 15014 (2015).
- [24] M. Goryachev, W. G. Farr, D. L. Creedon, Y. Fan, M. Kostylev, and M. E. Tobar, High-cooperativity cavity QED with magnons at microwave frequencies, *Phys. Rev. Appl.* **2**, 054002 (2014).
- [25] L. Bai, M. Harder, Y. P. Chen, X. Fan, J. Q. Xiao, and C.-M. Hu, Spin pumping in electro-dynamically coupled magnon-photon systems, *Phys. Rev. Lett.* **114**, 227201 (2015).
- [26] Y. Cao, P. Yan, H. Huebl, S. T. B. Goennenwein, and G. E. W. Bauer, Exchange magnon-polaritons in microwave cavities, *Phys. Rev. B* **91**, 094423 (2015).
- [27] B. Zare Rameshti, Y. Cao, and G. E. W. Bauer, Magnetic spheres in microwave cavities, *Phys. Rev. B* **91**, 214430 (2015).
- [28] B. M. Yao, Y. S. Gui, Y. Xiao, H. Guo, X. S. Chen, W. Lu, C. L. Chien, and C.-M. Hu, Theory and experiment on cavity magnon-polariton in the one-dimensional configuration, *Phys. Rev. B* **92**, 184407 (2015).
- [29] V. L. Grigoryan, K. Shen, and K. Xia, Synchronized spin-photon coupling in a microwave cavity, *Phys. Rev. B* **98**, 024406 (2018).
- [30] M. Harder, Y. Yang, B. M. Yao, C. H. Yu, J. W. Rao, Y. S. Gui, R. L. Stamps, and C.-M. Hu, Level attraction due to dissipative magnon-photon coupling, *Phys. Rev. Lett.* **121**, 137203 (2018).
- [31] B. Bhoi, B. Kim, S.-H. Jang, J. Kim, J. Yang, Y.-J. Cho, and S.-K. Kim, Abnormal anticrossing effect in photon-magnon coupling, *Phys. Rev. B* **99**, 134426 (2019).
- [32] W. Yu, J. Wang, H. Y. Yuan, and J. Xiao, Prediction of attractive level crossing via a dissipative mode, *Phys. Rev. Lett.* **123**, 227201 (2019).
- [33] X. Zhang, C.-L. Zou, N. Zhu, F. Marquardt, L. Jiang, and H. X. Tang, Magnon dark modes and gradient memory, *Nat. Commun.* **6**, 8914 (2015).
- [34] J. A. Haigh, N. J. Lambert, A. C. Doherty, and A. J. Ferguson, Dispersive readout of ferromagnetic resonance for strongly coupled magnons and microwave photons, *Phys. Rev. B* **91**, 104410 (2015).
- [35] X. Zhang, C.-L. Zou, L. Jiang, and H. X. Tang, Cavity magnomechanics, *Sci. Adv.* **2**, e1501286 (2016).
- [36] C. Braggio, G. Carugno, M. Guarise, A. Ortolan, and G. Ruoso, Optical manipulation of a magnon-photon hybrid system, *Phys. Rev. Lett.* **118**, 107205 (2017).
- [37] L. Bai, M. Harder, P. Hyde, Z. Zhang, C.-M. Hu, Y. P. Chen, and J. Q. Xiao, Cavity mediated manipulation of distant spin currents using a cavity-magnon-polariton, *Phys. Rev. Lett.* **118**, 217201 (2017).
- [38] D. Zhang, X.-Q. Luo, Y.-P. Wang, T.-F. Li, and J. Q. You, Observation of the exceptional point in cavity magnon-polaritons, *Nat. Commun.* **8**, 1368 (2017).
- [39] B. Zare Rameshti and G. E. W. Bauer, Indirect coupling of magnons by cavity photons, *Phys. Rev. B* **97**, 014419 (2018).
- [40] I. Boventer, M. Pfirrmann, J. Krause, Y. Schön, M. Kläui, and M. Weides, Complex temperature dependence of coupling and dissipation of cavity magnon polaritons from millikelvin to room temperature, *Phys. Rev. B* **97**, 184420 (2018).
- [41] Y. Cao and P. Yan, Exceptional magnetic sensitivity of \mathcal{PT} -symmetric cavity magnon polaritons, *Phys. Rev. B* **99**, 214415 (2019).
- [42] J. W. Rao, S. Kaur, B. M. Yao, E. R. J. Edwards, Y. T. Zhao, X. Fan, D. Xue, T. J. Silva, Y. S. Gui, and C.-M. Hu, Analogue of dynamic Hall effect in cavity magnon polariton system and coherently controlled logic device, *Nat. Commun.* **10**, 2934 (2019).
- [43] Y.-P. Wang, J. W. Rao, Y. Yang, P.-C. Xu, Y. S. Gui, B. M. Yao, J. Q. You, and C.-M. Hu, Nonreciprocity and unidirectional invisibility in cavity magnonics, *Phys. Rev. Lett.* **123**, 127202 (2019).
- [44] H. Y. Yuan, P. Yan, S. Zheng, Q. Y. He, K. Xia, and M.-H. Yung, Steady Bell state generation via magnon-photon coupling, *Phys. Rev. Lett.* **124**, 053602 (2020).
- [45] Y. Yang, Y.-P. Wang, J. W. Rao, Y. S. Gui, B. M. Yao, W. Lu, and C.-M. Hu, Unconventional singularity in anti-parity-time symmetric cavity magnonics, *Phys. Rev. Lett.* **125**, 147202 (2020).
- [46] A. Morin, C. Lacroix, and D. Ménard, Effect of dipolar interactions on cavity magnon polaritons, *Phys. Rev. B* **102**, 224421 (2020).
- [47] Y. Wang, W. Xiong, Z. Xu, G.-Q. Zhang, and J.-Q. You, Dissipation-induced nonreciprocal magnon blockade in a magnon-based hybrid system, *Sci. China Phys. Mech. Astron.* **65**, 260314 (2022).
- [48] J. Xu, C. Zhong, X. Han, D. Jin, L. Jiang, and X. Zhang, Floquet cavity electromagnonics, *Phys. Rev. Lett.* **125**, 237201 (2020).
- [49] N. Crescini, C. Braggio, G. Carugno, A. Ortolan, and G. Ruoso, Coherent coupling between multiple ferrimagnetic spheres and a microwave cavity at millikelvin temperatures, *Phys. Rev. B* **104**, 064426 (2021).
- [50] J. M. P. Nair, D. Mukhopadhyay, and G. S. Agarwal, Cavity-mediated level attraction and repulsion between magnons, *Phys. Rev. B* **105**, 214418 (2022).
- [51] V. L. Grigoryan and K. Xia, Pseudo-Hermitian magnon-polariton system with a three-dimensional exceptional surface, *Phys. Rev. B* **106**, 014404 (2022).
- [52] B. Yao, Y. S. Gui, J. W. Rao, Y. H. Zhang, W. Lu, and C.-M. Hu, Coherent microwave emission of gain-driven polaritons, *Phys. Rev. Lett.* **130**, 146702 (2023).
- [53] Y.-P. Wang, G.-Q. Zhang, D. Zhang, X.-Q. Luo, W. Xiong, S.-P. Wang, T.-F. Li, C.-M. Hu, and J. Q. You, Magnon Kerr effect in a strongly coupled cavity-magnon system, *Phys. Rev. B* **94**, 224410 (2016).
- [54] Y.-P. Wang, G.-Q. Zhang, D. Zhang, T.-F. Li, C.-M. Hu, and J. Q. You, Bistability of cavity magnon polaritons, *Phys. Rev. Lett.* **120**, 057202 (2018).
- [55] P. Hyde, B. M. Yao, Y. S. Gui, G.-Q. Zhang, J. Q. You, and C.-M. Hu, Direct measurement of foldover in cavity magnon-polariton systems, *Phys. Rev. B* **98**, 174423 (2018).
- [56] G. Zhang, Y. Wang, and J. You, Theory of the magnon Kerr effect in cavity magnonics, *Sci. China Phys. Mech. Astron.* **62**, 987511 (2019).
- [57] C. Kong, H. Xiong, and Y. Wu, Magnon-induced nonreciprocity based on the magnon Kerr effect, *Phys. Rev. Appl.* **12**, 034001 (2019).

- [58] M. Wang, C. Kong, Z.-Y. Sun, D. Zhang, Y.-Y. Wu, and L.-L. Zheng, Nonreciprocal high-order sidebands induced by magnon Kerr nonlinearity, *Phys. Rev. A* **104**, 033708 (2021).
- [59] J. M. P. Nair, D. Mukhopadhyay, and G. S. Agarwal, Ultra-low threshold bistability and generation of long-lived mode in a dissipatively coupled nonlinear system: Application to magnonics, *Phys. Rev. B* **103**, 224401 (2021).
- [60] J. M. P. Nair, D. Mukhopadhyay, and G. S. Agarwal, Enhanced sensing of weak anharmonicities through coherences in dissipatively coupled anti-PT symmetric systems, *Phys. Rev. Lett.* **126**, 180401 (2021).
- [61] H. Pan, Y. Yang, Z. H. An, and C.-M. Hu, Bistability in dissipatively coupled cavity magnonics, *Phys. Rev. B* **106**, 054425 (2022).
- [62] C. Zhao, Z. Yang, R. Peng, J. Yang, C. Li, and L. Zhou, Dissipative-coupling-induced transparency and high-order sidebands with Kerr nonlinearity in a cavity-magnonics system, *Phys. Rev. Appl.* **18**, 044074 (2022).
- [63] G.-Q. Zhang, Y. Wang, and W. Xiong, Detection sensitivity enhancement of magnon Kerr nonlinearity in cavity magnonics induced by coherent perfect absorption, *Phys. Rev. B* **107**, 064417 (2023).
- [64] R.-C. Shen, J. Li, Z.-Y. Fan, Y.-P. Wang, and J. Q. You, Mechanical bistability in Kerr-modified cavity magnomechanics, *Phys. Rev. Lett.* **129**, 123601 (2022).
- [65] J. M. P. Nair, Z. Zhang, M. O. Scully, and G. S. Agarwal, Nonlinear spin currents, *Phys. Rev. B* **102**, 104415 (2020).
- [66] M. X. Bi, X. H. Yan, Y. Zhang, and Y. Xiao, Tristability of cavity magnon polaritons, *Phys. Rev. B* **103**, 104411 (2021).
- [67] R.-C. Shen, Y.-P. Wang, J. Li, S.-Y. Zhu, G. S. Agarwal, and J. Q. You, Long-time memory and ternary logic gate using a multistable cavity magnonic system, *Phys. Rev. Lett.* **127**, 183202 (2021).
- [68] See Supplemental Material at <http://link.aps.org/supplemental/10.1103/PhysRevLett.132.137201> for additional details of the theoretical derivations, basins of attraction, nonlinear behaviors, control of folded hidden state, nonlinear transmission spectrum, impact of noise on hidden multistability, and hidden multistability in other nonlinear physical and biological systems, which includes Refs. [19–23,26,28,53,67,69–74].
- [69] D. F. Walls and G. J. Milburn, *Quantum Optics* (Springer, Berlin, 1994).
- [70] P. D. Drummond and D. F. Walls, Quantum theory of optical bistability. I. Nonlinear polarisability model, *J. Phys. A* **13**, 725 (1980).
- [71] J. R. Macdonald, Ferromagnetic resonance and the internal field in ferromagnetic materials, *Proc. Phys. Soc.* **64**, 968 (1951).
- [72] T. Holstein and H. Primakoff, Field dependence of the intrinsic domain magnetization of a ferromagnet, *Phys. Rev.* **58**, 1098 (1940).
- [73] I. S. Gradshteyn and I. M. Ryzhik, *Table of Integrals, Series, And Products* (Academic Press, Orlando, 1980).
- [74] L. De Mot, D. Gonze, S. Bessonard, C. Chazaud, A. Goldbeter, and G. Dupont, Cell fate specification based on tristability in the inner cell mass of mouse blastocysts, *Biophys. J.* **110**, 710 (2016).
- [75] A. N. Pisarchik and A. E. Hramov, *Multistability in Physical and Living Systems* (Springer, New York, 2022), Vol. 2.
- [76] K. Kaneko, Chaotic but regular posi-nega switch among coded attractors by cluster-size variation, *Phys. Rev. Lett.* **63**, 219 (1989).
- [77] V. Chizhevsky and S. Turovets, Small signal amplification and classical squeezing near period-doubling bifurcations in a modulated CO₂-laser, *Opt. Commun.* **102**, 175 (1993).
- [78] D. Dudkowski, S. Jafari, T. Kapitaniak, N. V. Kuznetsov, G. A. Leonov, and A. Prasad, Hidden attractors in dynamical systems, *Phys. Rep.* **637**, 1 (2016).